Synthesis of Photonic Microwave Filters Based on External Optical Modulators and Wide-Band Chirped Fiber Gratings

V. Polo, F. Ramos, J. Marti, D. Moodie, and D. Wake

***Abstract*—In this paper, the synthesis of photonic microwave filters employing optical sources with modulation side-bands, as multimode optical sources, and chirped fiber gratings is addressed. A single wavelength laser externally modulated using electrooptical Mach–Zehnder modulators and electroabsorption modulators have been proved as optical sources with modulation sidebands. Microwave filter features such as wide range tunability, compactness, readily reconfigurable frequency responses and flexibility have been achieved and demonstrated for the proposed structure. Experimental results using both a dual-electrode Mach–Zehnder electrooptical modulator and an electroabsorption modulator as optical sources with modulation sidebands are provided to demonstrate the feasibility of this technique.**

***Index Terms*—Chirped fiber gratings, electroabsorption modulators, filter synthesis, photonic microwave filters.**

I. Introduction

PHOTONIC microwave filters have resulted in much interest primary due to their large bandwidth, wide dynamic range and potential small packet size. Different techniques based on dispersive fiber delay lines have been proposed, such as a fiber optic prism fed by a tunable laser [1], a multiple uncorrelated wavelength source by combining tunable lasers feeding a highly dispersive fiber [2] and a broad-band spectrum-sliced optical source launched also into a dispersive fiber [3]. Furthermore, wide-band chirped fiber gratings (CFG) have been demonstrated as high-performance optical delay lines [4] and their application to photonic microwave filters using multimode optical sources [5], [6]. In [6], an optical source with modulation sidebands (OSMS's) was implemented by sinusoidally modulating a DFB laser through an external electroabsorption modulator (EAM). Such modulation scheme produces modulation sidebands (frequency modes), which are evenly spaced, in the optical domain, by the frequency of the modulating signal, producing a spectral shape similar to that of a multimode source. In order to achieve a wide tunability range and a flexible reconfigurable filter frequency response as well as low insertion loss and compactness, two alternative implementations of the OSMS have been proved. A single wavelength optical source followed by an external modulator, which can be either an electroabsorption modulator [6] or a Mach–Zehnder electrooptical modulator (MZ-EOM), driven by a local oscillator (LO) signal is used as flexible multimode optical source.

In this paper, a generalized synthesis procedure of photonic microwave filters using wide-band CFG as dispersive elements and a multimode optical source is presented. Practical realizations of microwave filters using EAM-based and MZ-EOM-based OSMS are presented. It is shown experimentally that the EAM configuration allows more flexibility than that using MZ-EOM's since by varying the EAM bias voltage and the LO frequency different microwave filter responses may be readily synthesized. The paper is organized as follows. In Section II the general principle of operation of photonic microwave filters based on CFG and multimode optical sources is addressed. This analysis is also valid if OSMS are considered, by simply substituting longitudinal modes by frequency modes. Due to the higher flexibility provided by the EAM-based optical source a generalized spectral synthesis analysis using this source is presented in Section III. Two practical realizations of microwave filters employing MZ-EOM's and EAM's, both driven by a LO signal, are implemented in Section IV providing experimental results. Finally, in Section V the conclusions of the paper are presented.

II. General Principle

The general setup of the photonic microwave filter proposed structure is depicted in Fig. 1. A multimode optical source is externally modulated by a radio-frequency (RF) input signal and it is further transmitted through a dispersive medium prior to photodetection. This dispersive medium induces different delays over each longitudinal mode (LM) of the optical source, leading to a filtering of the RF signal as a consequence of the summation of the different field components that occurs at the photodetector.

The complex amplitude of the optical field at the output of the MZ-EOM, $E(t)$, may be expressed as

$$E(t) \propto \sqrt{1+m\cos(2\pi f_{\mathrm{RF}}t)}\,\exp(j2\pi f_0 t) \cdot \sum_n E_n \exp[j(2\pi n\nu t+\phi_n)] \tag{1}$$

where

m modulation depth;

f_{RF} frequency of the input signal;

Manuscript received June 7, 1999; revised November 15, 1999. This work was supported by the Spanish Research Commission (CICYT) Project #TIC96-0611

V. Polo, F. Ramos, and J. Marti are with ETSI Telecomunicacion, Universidad Politecnica de Valencia, Camino de Vera s/n, 46022 Valencia, Spain (e-mail: jmarti@dcom.upv.es).

D. Moodie and D. Wake are with BT Laboratories, Martlesham Heath, Ipswich, Suffolk, IP5 3RE, U.K.

Publisher Item Identifier S 0733-8724(00)01315-3.

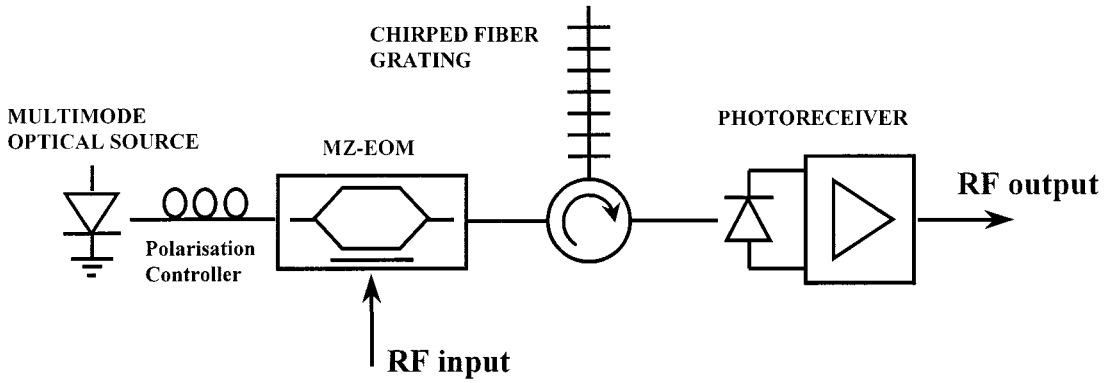

Fig. 1. Setup of a photonic microwave filter employing a multimode optical source and chirped fiber gratings.

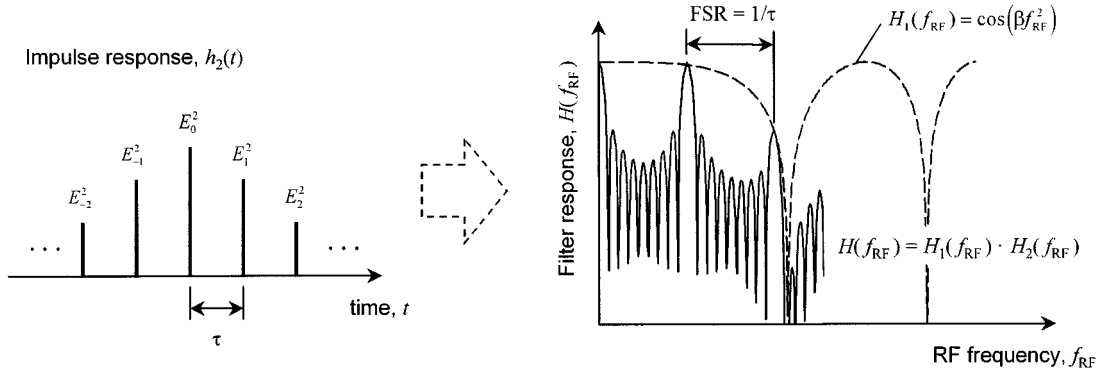

Fig. 2. Schematic about the relations between the optical parameters of the system and the obtained filter response. $H_2(f_{\rm RF})$ is the Fourier transform of the sequence $\{E_n^2\}$.

f_0 carrier optical frequency;
E_n amplitude phase of the nth LM;
ϕ_n relative phase of the nth LM;
ν optical frequency separation between them.

Next, this field is transmitted through a CFG characterized by a total first-order dispersion parameter, D_T, in ps/nm and photodetected to recover the RF signal. Thus, after some mathematical manipulations, the overall optical processing of the RF signal may be characterized by an electrical transfer function

$$H(f_{\rm RF}) \propto \cos(\beta f_{\rm RF}^2) \sum_n E_n^2 \exp(j2n\upsilon\beta f_{\rm RF}) \qquad (2)$$

where $\beta = \pi c D_T / f_0^2$. The first term in (2) is the well-known dispersion-induced power degradation as a result of propagation of the RF signal through the dispersive media, which may be compensated employing single-side band (SSB) modulation at the MZ-EOM [7]. From now, this envelope term will be omitted in the discussions. The second term in (2) corresponds to the optical transversal filter impulse response, given by

$$h_2(t) = \sum_n E_n^2 \delta\left(t - n\frac{\beta\nu}{\pi}\right). \qquad (3)$$

The relationship between the optical parameters and the microwave filter response is shown schematically in Fig. 2. Note that the weights of the impulse response in (3) are always positive and do not depend on the relative phases of the LM's. Therefore, this scheme, as is, does not allow to synthesize high-pass filters. Finally, the free-spectral range (FSR) of the filter is calculated as

$$\text{FSR} = \frac{\pi}{\beta\upsilon} = \frac{f_0^2}{cD_T\nu}. \qquad (4)$$

The FSR of the filter is related to its tunability, while the field amplitudes of the LM's of the optical source are also related to the shape of the filter response. Therefore, different windowing

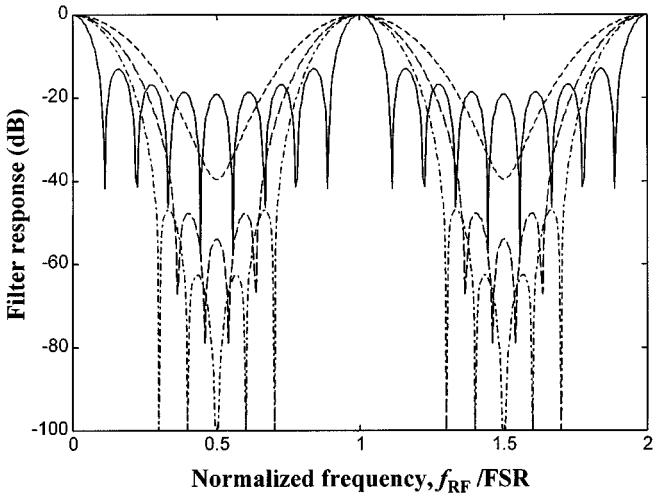

Fig. 3. Filter response as a function of the normalized frequency $f_{\rm RF}$/FSR for different windowing functions of the coefficients E_n. Solid line: uniform, short-dashed line: Blackmann, dashed line: Hamming, and dashed-dotted line: Hanning.

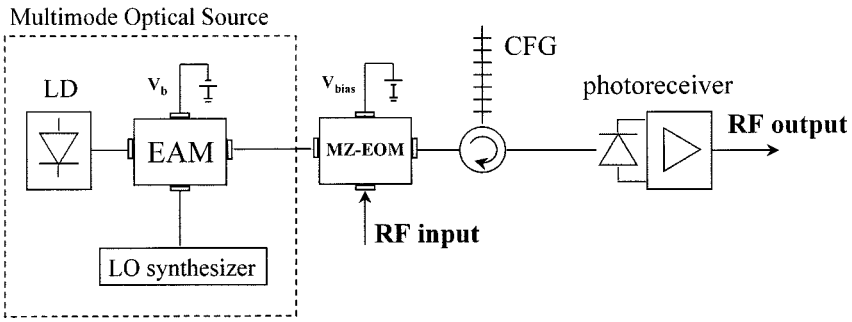

Fig. 4. Setup of the photonic microwave filter using and EAM for the generation of the multimode optical signal.

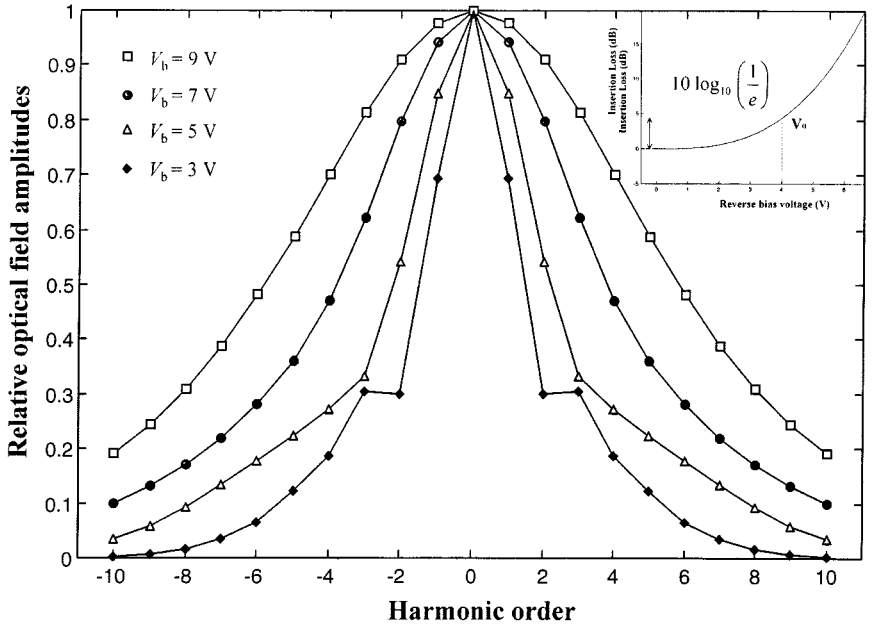

Fig. 5. Field spectrum for several values of the bias voltage applied to the EAM. The field amplitudes are normalized to the maximum and the harmonic order is the index n of (1). The inset shows the theoretical insertion loss of an EAM with $a = 3$ and $V_0 = 4$ V, following (5).

functions for the coefficients E_n produce different bandwidths and sidelobe amplitudes [8]. The filter response for several windowing functions is compared in Fig. 3, in which the solid line corresponds to an uniform window, the short-dashed line is for a Blackmann window, the dashed line was obtained for the Hamming function, and finally the dash-dotted line corresponds to a Hanning window. In all cases we have supposed a multimode optical source with nine significative LM's. As in electronic digital filters [8], the sharpest selectivity response was provided by the uniform window, while the worst selectivity was for the Blackmann one. However, the side-lobe amplitudes are much better for the Hanning window (< -40 dB) than for the uniform one (< -15 dB).

III. Spectral Synthesis Employing Electroabsorption Modulators

The spectral output of the OSMS mainly determines the photonic microwave filter shape, as deduced in (2). Several approaches and devices have been used to generate OSMS such as multiple tunable laser source [2], broadband optical source with sliced-spectrum [3], Fabry–Perot (FP) laser diodes [5], and mode-locked lasers [9]. In this paper, an efficient and compact approach for implementing the OSMS based on the use of an EAM driven by a LO signal is considered. In fact, commercially

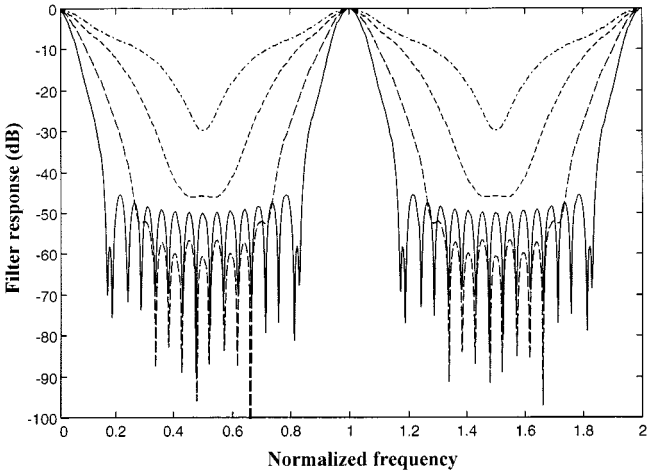

Fig. 6. Filter responses for several values of the bias voltage applied to the EAM and for $\alpha = 3$. $V_b = 3$ V (dashed–dotted line), $V_b = 5$ V (short-dashed line), $V_b = 7$ V (dashed line), and $V_b = 9$ V (solid line).

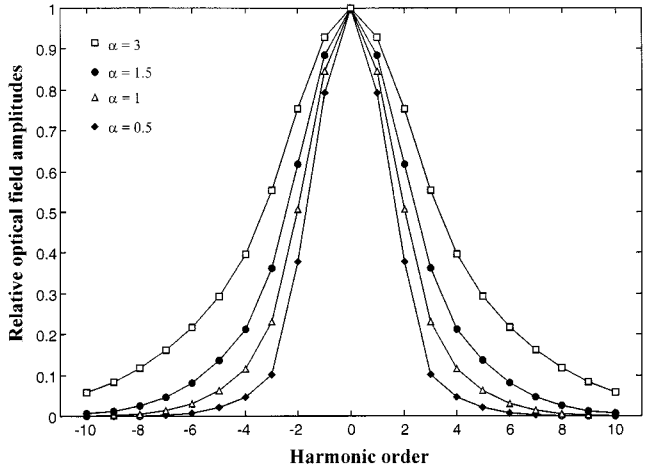

Fig. 7. Field spectrum for several values of the α-parameter of the EAM. The field amplitudes are normalized to the maximum and the harmonic order is the index n of (1).

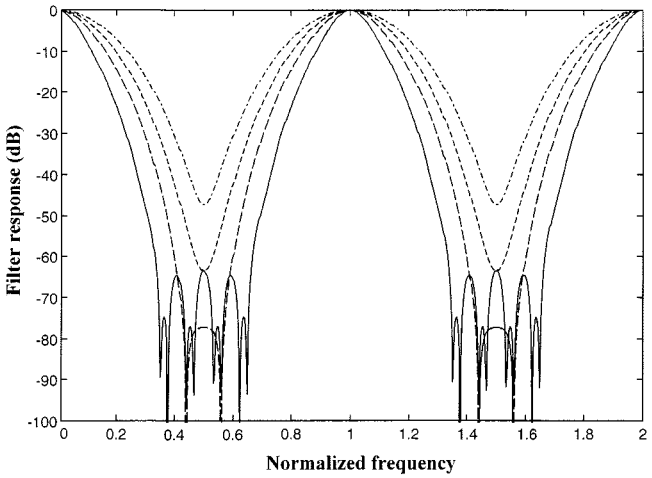

Fig. 8. Filter responses for several values of the α-parameter of the EAM and for $V_b = 7$ V. $\alpha = 0.5$ (dashed–dotted line), $\alpha = 1$ (short-dashed line), $\alpha = 1.5$ (dashed line), and $\alpha = 3$ (solid line).

available distributed feedback lasers/EAM integrated modules would be very useful. The proposed setup is shown in Fig. 4. The output of a single wavelength laser diode is externally modulated by a millimeter-wave signal at frequency $f_{\rm LO}$ using an EAM. The optical power at the output of the EAM, $P_{\rm out}$, may be modeled as

$$P_{\rm out} = P_0 \exp\left[-(V_{\rm LO}/V_0)^a\right] \tag{5}$$

where

P_0	effective optical power of the input light including the insertion losses of the modulator;
V_0 and a	constants (typical values for a are 1–2 for Franz–Keldish modulators and 2–4 for multiple quantum-well modulators [10]);
$V_{\rm LO}$	applied voltage which may be expressed as

$$V_{\rm LO} = V_b(1 + m_{\rm LO} \cos 2\pi f_{\rm LO} t) \tag{6}$$

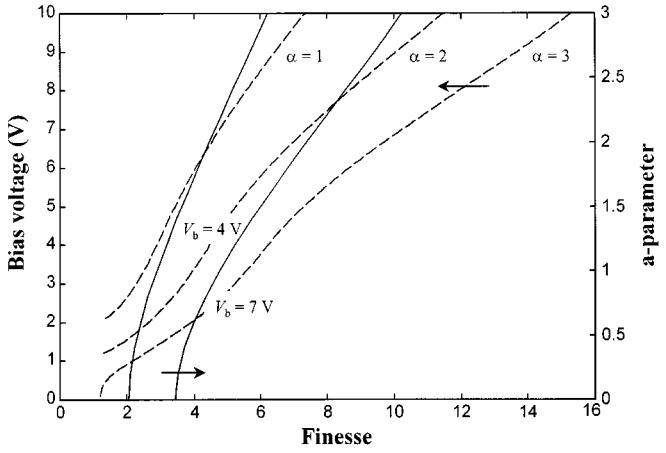

Fig. 9. Needed values of the bias voltage or the α-parameter of the EAM for a given finesse of the filter. The solid lines are for two different bias voltages and varying the chirp, while the dashed-lines are for three different values of the α-parameter and varying the bias voltage. Other parameters of the EAM are $a = 3$, $V_0 = 4$ V, and $P_{\rm LO} = +20$ dBm.

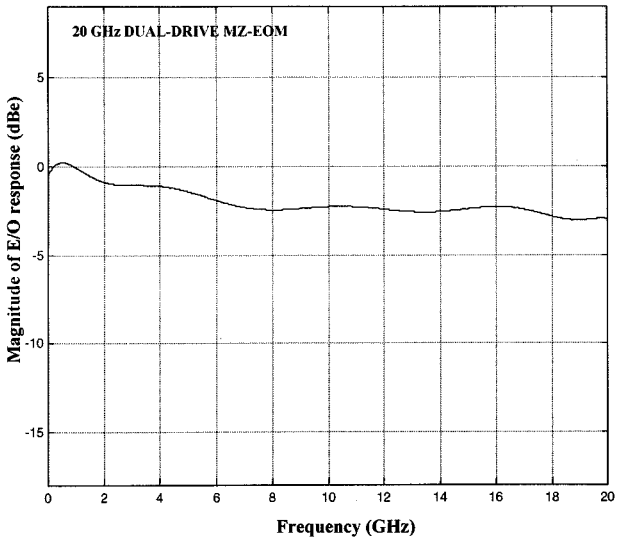

(a)

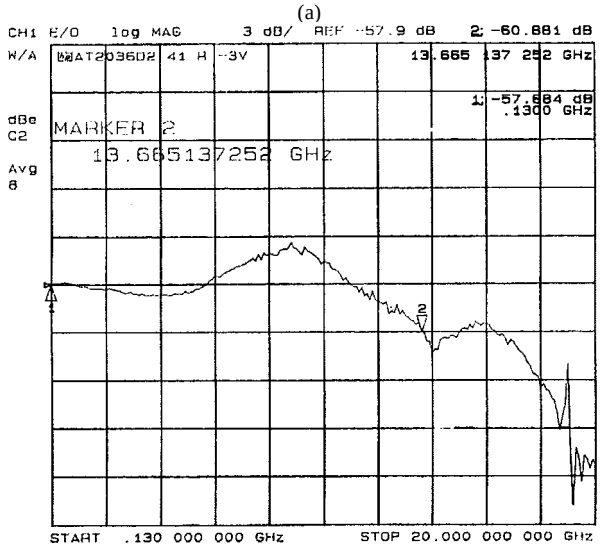

(b)

Fig. 10. Magnitude of E/O responses of the modulators employed in the experiments: (a) dual-drive MZ-EOM and (b) EAM. -3-dB bandwidths are 20 and 14 GHz, respectively.

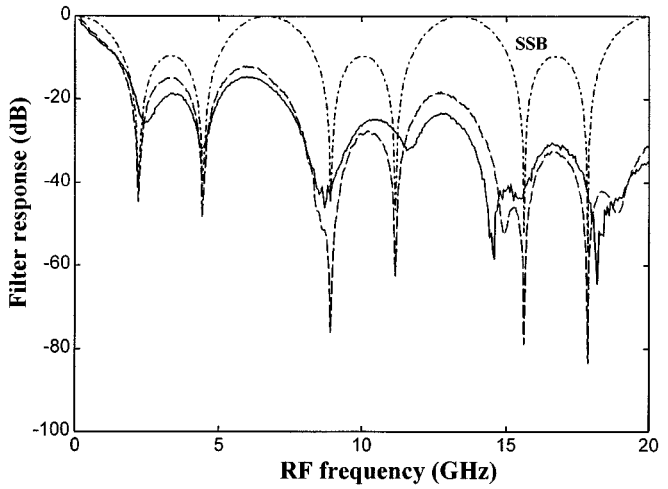

Fig. 11. Filter response employing a tunable laser and a dual-drive MZ-EOM operating at the minimum transmission point as multimode optical source. The modulating frequency of the MZ-EOM was 20 GHz. The solid line is the measurement, the dashed line is the theory including the frequency roll-off of the modulator and photodetector, and the dashed–dotted line is the theory for ideal SSB modulation.

V_b being the bias voltage and $m_{\rm LO} = \sqrt{2Z_{\rm in}P_{\rm LO}}/V_b$ the modulation index, where

$Z_{\rm in}$ input impedance of the RF electrode;

$P_{\rm LO}$ local oscillator power.

Due to the nonlinear response of the EAM, as denoted in (5), its output optical field consists of several equally spaced spectral components with a separation $\nu = f_{\rm LO}$. The expression of the optical field is [11]

$$E_{\rm out}(t) = P_{opt}^{\gamma} \exp(j2\pi f_0 t) \tag{7}$$

where $\gamma = (1 + j\alpha)/2$, α being the chirp parameter of the modulator [12]. The relative amplitudes of the LM's for a given EAM depend on the bias point, V_b, the local oscillator power, $P_{\rm LO}$, and the α-parameter. Moreover, a variation of V_b will further affect to: a) the contrast ratio of the output signal, and b) the α-parameter [13], [14]. The output of the OSMS is now modulated by the RF filter input signal employing a MZ-EOM biased for linear operation and its output impinges the CFG (dispersive medium) prior to photodetection. The variation of the modulation sideband amplitudes of the EAM ($a = 3$, $V_0 = 4$ V, $P_{\rm LO} = +20$ dBm, $\alpha = 3$), obtained by simulation, as a function of the biasing voltage is depicted in Fig. 5. The inset shows the dependence of the insertion loss on the reverse bias voltage of an EAM with such parameters, following (5). The point in which the insertion loss equals $1/e$ (V_0) has also been remarked. The photonic microwave filter responses generated by the EAM outputs plotted in Fig. 5 are shown in Fig. 6. From Figs. 5 and 6 it may be observed that higher reverse bias voltages produce narrower -3 dB filter bandwidths and sharper filter responses. Moreover, in Fig. 6 it can be seen that, in general, the filter response contrast ratio (peak-to-valley ratio) increases for higher reverse bias voltage, even though a change is this trend is observed for bias voltage higher than $V_b = 9$ V. It should be noticed that by varying the EAM bias point the α-parameter would change in a realistic device. In this section, we have assumed that it remains constant to isolate the influence of the reverse bias variation on the filter response. Experimental results obtained for a realistic α-parameter variation with reverse bias voltage are presented later in Section IV.

In Fig. 7, the relative optical field amplitudes of the first ten harmonics at the output of the EAM ($a = 3$, $V_0 = 4$ V, $P_{\rm LO} = +20$ dBm, $V_b = 7$ V) against the α-parameter are shown and their corresponding filter responses are depicted in Fig. 8. From the results of Figs. 7 and 8 it may be deduced that for higher α-parameters narrower filter bandwidths and sharper filter responses are achieved. As in Figs. 5 and 6, the trend of the contrast ratio also changes for higher bias voltages, as depicted in Fig. 8.

For a microwave filter synthesis purpose it is important to establish the relationships among the parameters of the desired filter response (e.g., FSR, -3-dB bandwidth, selectivity, etc.) and the physical parameters of the electrooptical structure (e.g., $f_{\rm LO}$, D_T, $P_{\rm LO}$, etc.). It has been shown that the FSR is directly related to the modulating frequency of the EAM, as described in (4). However other parameters such as the filter finesse, defined as F = FSR/(-3-dB bandwidth), do not have closed expressions. In this case, the results have been obtained by means of simulation and are depicted in Fig. 9. In this figure, the values of the bias voltage and the EAM α-parameter to achieve a given filter finesse are shown. The use of the results depicted in Fig. 9 is twofold. First, by fixing a α-parameter (dashed lines) the reverse bias voltage may be obtained for a certain filter finesse. Secondly, by fixing a reverse bias voltage (solid lines) the α-parameter may be found to achieve certain filter finesse. For example, if a microwave filter with an FSR of 5 GHz and a finesse of eight was specified, for a CFG dispersion slope of 910 ps/nm and a wavelength of 1550 nm, (4) gives a modulating frequency $f_{\rm LO} = 27.4$ GHz. Next, Fig. 9 provides the possible values of the chirp and the bias voltage of the EAM: $\alpha = 2$ and $V_b = 7.5$ V or $\alpha = 3$ and $V_b = 5.5$ V. Anyone of these two pairs of parameters may be used.

IV. Practical Realizations

In the previous section we have addressed theoretically the synthesis of photonic microwave filters employing EAM's. For the sake of comparison, experimental results are provided for two OSMS: one using a dual-electrode MZ-EOM and that based on an EAM. Fig. 10 shows the measured electooptical responses of both modulators used in the experiments: a 20-GHz -3-dB bandwidth dual-drive MZ-EOM (left) and a 14-GHz -3-dB bandwidth EAM. It is important to notice that the inevitable ripple in the electrooptical response of the modulator will induce undesired ripple in the synthesized filter responses. In both cases, we have measured the electrical transfer function of the filter employing a lightwave component analyzer. A 4 nm wide/40-cm-long CFG with a group delay slope of nearly 900 ps/nm was used. For the MZ-EOM-based source, a LO tone of 20 GHz with a power of $+20$ dBm was used in this experiment. The measured filter response employing the dual-electrode MZ-EOM and the CFG is shown in Fig. 11 (solid lines). In this case, the MZ-EOM was biased at the minimum transmission

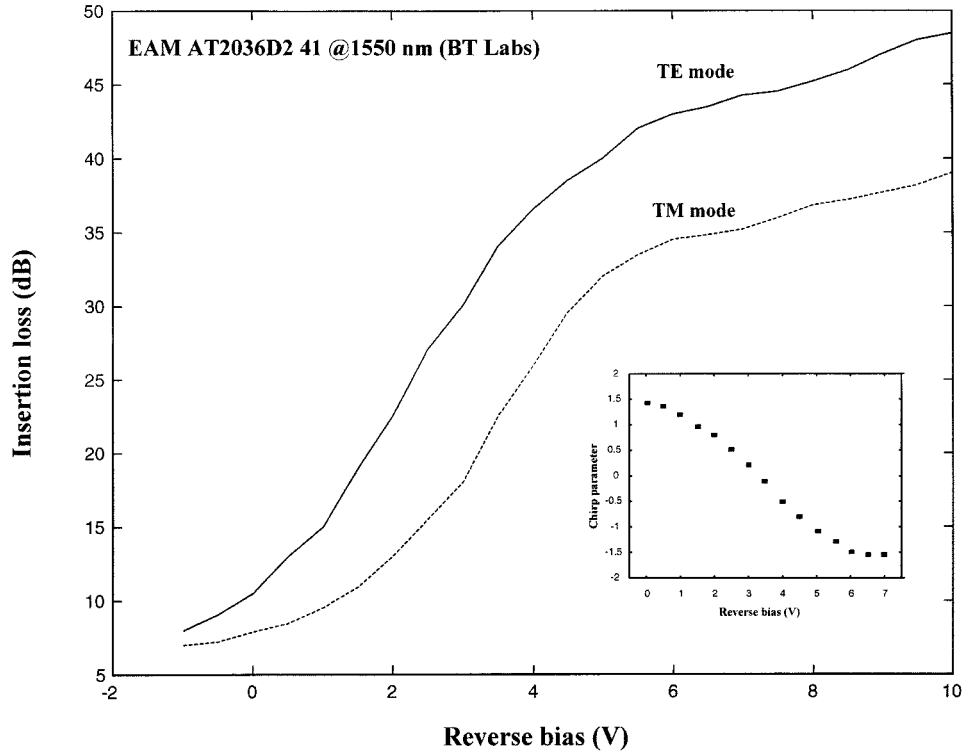

Fig. 12. EAM insertion loss as a function of the reverse bias voltage for TE and TM polarization states of the input light. The inset shows the measured EAM α-parameter versus the reverse bias voltage.

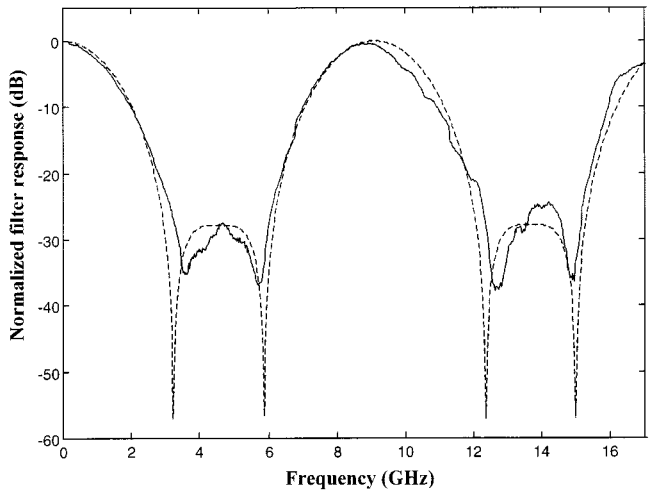

Fig. 13. Filter response employing a tunable laser and an EAM as multimode optical source. The modulating frequency of the EAM was 16 GHz and its reverse bias voltage was 3 V. The solid line is the measurement and the dashed line is the simulation.

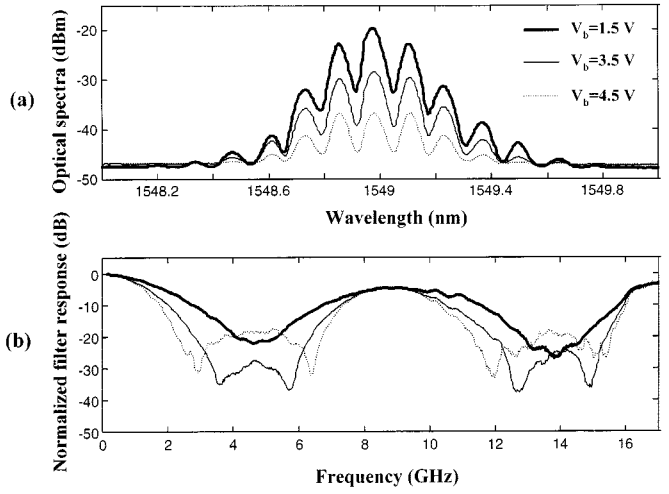

Fig. 14. (a) Measurements of the optical spectra at the EAM output for different reverse bias voltages. (b) Frequency response of the filter for different reverse bias voltages.

point and modulated with a RF tone of 20 GHz. This filter response includes the effects of the roll-off of the MZ-EOM and the photoreceiver as well as the power penalty envelope due to the dispersion of the CFG. Theoretical results are also depicted in Fig. 11 (dashed line) and a very good agreement with the measurements is observed. Moreover, theoretical results of the transversal filter response assuming an ideal SSB modulation of the RF input signal are also shown in Fig. 11 (dashed–dotted line). The low selectivity and high adjacent lobes of the filter response shown in Fig. 11 is due to the contribution of only three relevant frequency modes.

In the second type of practical microwave filter implementations an EAM-based OSMS was used. Fig. 12 depicts the measured insertion loss versus reverse bias voltage response of the EAM, both for TE and TM input optical field polarizations. Also the variation of α-parameter with the reverse bias is shown in the inset ($\lambda = 1550$ nm, TM polarization), measured using the method proposed in [14]. The simulated (dashed line) and experimental (solid line) filter responses are depicted in Fig. 13,

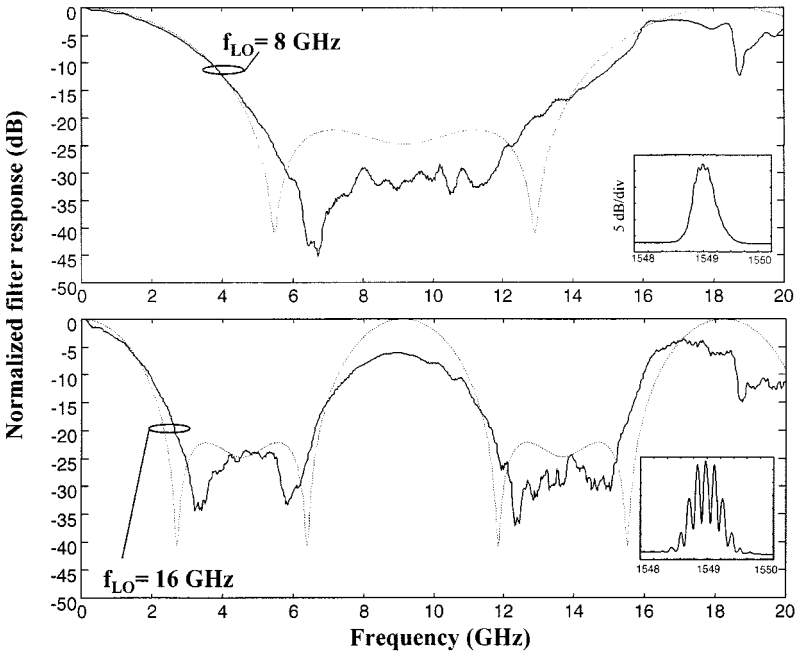

Fig. 15. Effects of the EAM modulating frequency on the FSR of the filter response. Solid lines correspond to the measured filter responses when modulating frequency tones of (a) 8 GHz (FSR = 18 GHz) and (b) 16 GHz (FSR = 9 GHz) are employed. Dashed lines correspond to the simulated filter responses.

showing a very good agreement between them. To obtain these results, the EAM was driven by a +20 dBm/16 GHz frequency tone leading to a filter response centered at nearly 9 GHz with a −3-dB bandwidth of 2 GHz. The EAM reverse bias voltage was set at 3 V. The DFB laser output power was +3 dBm. In Fig. 11, it can be seen that the rejection ratio (peak-to-valley ratio) outside the passband of the filter is nearly 30 dB. This figure shows a very good performance of these filters when compared with to other techniques [2], mainly due to the correlation of the modulation sidebands produced by the EAM-based OSMS. TM input light polarization was chosen to minimize optical insertion losses.

To demonstrate the impact of the spectral envelope of the optical modulation sidebands generated by the EAM on the filter response, the EAM reverse bias voltage was varied. Fig. 14(a) depicts the measured optical spectra at the output of the EAM for different reverse bias voltages, and the corresponding filter responses are depicted in Fig. 14(b). In Fig. 14, it may be observed that a higher frequency selectivity may be obtained by adjusting the EAM reverse bias voltage to broaden the envelope of the optical spectrum generated by the EAM, which is consistent with the classical theory of digital filter design [8]. However, the rejection ratio of the filter may be optimized by selecting a certain EAM reverse bias voltage. Finally, for a filter tuning purpose, the relationship between the frequency of the modulating tone and the filter FSR was experimentally demonstrated. Fig. 15 shows the measured filter responses when the EAM is modulated by an 8 GHz frequency tone [Fig. 13(a)] and a 16 GHz frequency tone [Fig. 15(b)] with a RF power of +20 dBm in both cases. The obtained FSR were nearly 18 GHz and 9 GHz, respectively. These values are in good agreement with the predicted theoretical ones deduced from (4), 17.8 and 8.7 GHz, respectively. The EAM reverse bias voltage was set to 4 V and the output power of the DFB was +3 dBm. In Fig. 15, it can be seen that the agreement between the theoretical approach and the experimental results is quite good. However, in Fig. 15(a) higher discrepancies may be observed for frequencies above 8 GHz. This is due to the high EAM-induced optical insertion losses (>25 dB, for $V_b = 4$ V), the 14 GHz electrical bandwith of the modulator and to the carrier suppression effect which appears as non-SSB modulation of the RF signal is employed. Also the value of D_T employed in (2), which does not correspond exactly with that of the CFG, may affect these differences. It should be pointed out that the EAM optical insertion loss increases as it does the reverse bias voltage. This implies that the optical power impinging the photodiode (PD) decreases, as shown by the optical spectra depicted in Fig. 14(a) which implies in turn that the signal-to-noise ratio (SNR) is reduced, if received input power-dependent noise contributions are not dominant. This must be taken into account in the filter design, but is out of the scope of this paper. In addition, the design technique presented in [15] allows customizing the chirp feature of the EAM independently of the extinction ratio, which implies that it is possible to achieve high negative α-parameters with lower optical insertion loss. The insets of Fig. 15 show the corresponding measured optical spectra. The results shown in Figs . 13–15 demonstrate that the photonic-microwave filter responses may be readily reconfigured by adjusting the EAM reverse bias voltage and the separation of the optical modes generated at its output.

V. Conclusion

It is proposed and experimentally demonstrated a compact photonic microwave filter structure employing an optical source with modulation sidebands and a wide-band CFG. The tuning feature of the filter must be accomplished by controlling the frequency spacing between modulation sidebands in the OSMS or

by varying the group delay slope in the CFG. Experimental results using a dual-electrode MZ-EOM and an EAM as OSMS have been presented. The EAM-based structure provides better filter performance than that employing the MZ-EOM with regard to sidelobe suppression ratio due to its intrinsic higher nonlinearity as well as it provides more flexibility and a readily reconfigurable filter architecture.

It has been theoretically and experimentally shown that an EAM could be employed as an efficient OSMS for implementing photonic microwave filters. The filter response shape and contrast ratio could be suited by varying the parameters of the modulator (α, V_b, and a), while the filter FSR is determined by the frequency of the electrical signal impinging the EAM or the group delay slope of the CFG. As recently shown in [15], it is possible to customize the chirp characteristics of an EAM independently of the extinction ratio. This allows the fabrication of an EAM suited to provide a desired photonic-microwave filter response.

ACKNOWLEDGMENT

The authors would like to acknowledge Generalitat Valenciana for providing the test equipment used in this work.

REFERENCES

[1] M. Y. Frankel and R. D. Esman, "Fiber optic tunable microwave transversal filter," *IEEE Photon. Technol. Lett.*, vol. 7, pp. 191–193, 1995.

[2] D. Norton, S. Johns, C. Keefer, and R. Soref, "Tunable microwave filter using high dispersion fiber time delays," *IEEE Photon. Technol. Lett.*, vol. 6, pp. 831–832, 1994.

[3] A. P. Foord, P. A. Davies, and P. A. Greenhalgh, "Synthesis of microwave and millimeter-wave filters using optical spectrum-sliced," *Electron. Lett.*, vol. 32, pp. 390–391, 1996.

[4] J. L. Corral, J. Marti, S. Regidor, J. M. Fuster, R. I. Laming, and M. J. Cole, "Continuously variable true time-delay optical feeder for phased-array antenna employing chirped fiber gratings," *IEEE Trans. Microwave Theory Tech.*, vol. 45, pp. 1531–1536, 1997.

[5] J. Marti, F. Ramos, and R. I. Laming, "Photonic microwave filter employing multimode optical sources and wideband chirped fiber gratings," *Electron. Lett.*, vol. 34, pp. 1760–1761, 1998.

[6] J. Marti, V. Polo, F. Ramos, and D. Moodie, "Photonic tunable microwave filters employing electroabsorption modulators and wideband chirped fiber gratings," *Electron. Lett.*, vol. 35, pp. 305–306, 1999.

[7] J. L. Corral, J. Marti, J. M. Fuster, and R. I. Laming, "Dispersion-induced bandwidth limitation of variable true time-delay lines based on linearly chirped fiber gratings," *Electron. Lett.*, vol. 34, pp. 209–211, 1998.

[8] A. Oppenheim and R. Schaffer, *Discrete-Time Signal Processing*. Englewood Cliffs, NJ: Prentice-Hall, 1989.

[9] D. Novak, Z. Ahmed, R. B. Waterhouse, and R. S. Tucker, "Signal generation using pulsed semiconductor lasers for application in millimeter-wave wireless links," *IEEE Trans. Microwave Theory Tech.*, vol. 43, pp. 2257–2262, 1995.

[10] O. Mitomi, K. Wakita, and I. Kotaka, "Chirping characteristic of electroabsorption-type optical-intensity modulator," *IEEE Photon. Technol. Lett.*, vol. 6, pp. 205–207, Feb. 1994.

[11] O. Mitomi, S. Nojima, I. Kotaka, K. Wakita, K. Kawano, and M. Naganuma, "Chirping characteristic and frequency response of MQW optical intensity modulator," *J. Lightwave Technol.*, vol. 10, pp. 71–76, Jan. 1992.

[12] F. Koyoma and K. Iga, "Frequency chirping in external modulators," *J. Lightwave Technol.*, vol. LT-6, pp. 87–92, 1988.

[13] J. C. Cartledge and B. Christensen, "Optimum operating points for electroabsorption modulators in 10 Gb/s transmission systems using nondispersion shifted fiber," *J. Lightwave Technol.*, vol. 16, pp. 349–357, Mar. 1998.

[14] F. Devaux, Y. Sorel, and J. F. Kerdiles, "Simple measurement of fiber dispersion of chirp parameter of intensity modulated light emitter," *J. Lightwave Technol.*, vol. 11, pp. 1937–1940, Dec. 1993.

[15] M. Matsuda, "A novel method for designing chirp characteristics in electroabsorption MQW optical modulators," *IEEE Photon. Technol. Lett.*, vol. 10, pp. 364–366, Mar. 1998.

V. Polo (S'93) was born in Valencia, Spain, in 1972. He received the Ingeniero Superior de Telecomunicacion degree from the Universidad Politecnica de Valencia in 1997. He is currently pursuing the Ph.D. degree at the same university.

Presently, he is a member of the Fibre–Radio Group at the Universidad de Valencia. His research interests include applications of electrooptical and electroabsorption modulators in microwave and millmeter-wave radio-over-fiber systems, dispersion compensation, and broad-band access systems and technologies including WLL, LMDS, DWDM-SCM, FTTx, HFC, and PON. He has co-authored over 20 papers in international journals and conferences.

Mr. Polo is a student member of several IEEE societies.

F. Ramos was born in Valencia, Spain, on April 2, 1974. He received the Ingeniero Superior de Telecomunicacion degree from the Universidad Politecnica de Valencia in 1997. He is currently pursuing the Ph.D. degree at the same university.

Presently, he is a member of the Fibre–Radio Group at the Universidad de Valencia. His research interests include nonlinear fiber optics, compensation of intensity noise and nonlinear distortion due to the optical fiber, optical-phase conjugation, and microwave and millmeter-wave optical systems.

Mr. Ramos has been a Reviewer of the *Journal of Fiber and Integrated Optics*. He is the recipient of the Prize of the Telecommunication Engineering Association of Spain for his study on compensation of fiber-induced nonlinear distortion in CATV systems employing optical-phase conjugation.

J. Marti (S'89–M'93) received the Ingeniero Tecnico de Telecomunicacion and the Ingeniero de Telecomunicacion degrees from the Universidad Politecnica de Catalunya, Spain, in 1988 and 1991, respectively. He received the Ph.D. (Doctor Ingeniero de Telecomunicacion) degree from the Universidad Politecnica de Valencia, Spain, in 1994.

During 1989 and 1990, he was an Assistant Lecturer at the Escuela Universitaria de Vilanova, Barcelona, Spain. He joined the Departamento de Comunicaciones at the Universidad Politecnica de Valencia, in 1991. From 1991 to 1994, he was a Lecturer at the Telecommunication Engineering Faculty and he has been an Associate Professor since 1995. Currently, he is leading the Fibre–Radio Group at the same university. He has published over 70 papers in refereed international technical journals and 30 papers in international conferences in the fields of fiber-radio and microwave/millimeter-wave photonics, WDM, and SCM lightwave systems, optical processing of microwave signals, dispersion, and fiber nonlinearities compensation employing fiber gratings and other techniques, and mobile and satellite communications systems. His current technical interests include microwave/millimeter-wave fiber-radio systems and DWDM hybrid fiber-radio access techniques and networks.

Dr. Marti is a member of the Technical Committee of ECOC, and some other international workshops and conferences.

D. Moodie, photograph and biography not available at the time of publication.

D. Wake, photograph and biography not available at the time of publication.